Robust Superhydrophobic Membrane for Membrane Distillation with Excellent Scaling Resistance

Chunlei Su [a,b,c], Thomas Horseman [d], Hongbin Cao [b], Kofi Christie [a], Yuping Li [b*], Shihong Lin [a,d*]

[a] Department of Civil and Environmental Engineering, Vanderbilt University, Nashville, Tennessee 37235-1831, United States

[b] Beijing Engineering Research Centre of Process Pollution Control, Institute of Process Engineering, Chinese Academy of Sciences, Beijing 100190, China

[c] University of Chinese Academy of Sciences, Beijing 100049, China

[d] Department of Chemical and Biomolecular Engineering, Vanderbilt University, Nashville, Tennessee 37235-1831, United States

*Corresponding author.

E-mail:ypli@ipe.ac.cn Phone: + 86 1082544839. (Y. L.)

E-mail:shihong.lin@vanderbilt.edu. Phone: +1 (615) 322-7226. (S.L.)

ABSTRACT

We report in this study a scalable and controllable approach for fabricating robust and high-performance superhydrophobic membranes for membrane distillation (MD). This novel approach combines electro-co-spinning/spraying (ES^2) with chemical vapor welding, and enables the formation of robust superhydrophobic (r-SH) membranes that are mechanically strong, highly porous, and robustly superhydrophobic. Compared with superhydrophobic membranes obtained using surface deposition of fluorinated nanoparticles, the r-SH membranes have more robust wetting properties and higher vapor permeability in MD. MD scaling experiments with NaCl and gypsum show that the r-SH membrane is highly effective in mitigating mineral scaling. Finally, we also discuss the mechanism of scaling resistance enabled by superhydrophobic membranes with a highlight on the roles of the surface-bound air layer in reducing the crystal-membrane contact area, nucleation propensity, and ion-membrane contact time.

INTRODUCTION

Membrane distillation (MD), which can harvest low-grade waste heat for desalinating high salinity brine, is potentially a promising solution for hypersaline brine management in oil and gas wastewater treatment and zero liquid discharge [1, 2]. In a typical MD process, the temperature difference between hot salty water (the feed solution) and cold deionized water (the distillate) results in a partial vapor pressure difference that drives the vapor to transport from the feed stream to the distillate stream, thereby producing distilled water [3-7].

If MD is applied for hypersaline brine treatment, membrane scaling represents a major and unavoidable technical challenge as the feed streams will eventually become oversaturated [8]. The formation of mineral scales can induce both fouling, which reduces water vapor flux, and pore wetting, which reduces salt rejection, either of which will compromise the performance and eventual fail the MD process. Extensive research has been performed to explore strategies for scaling mitigation in MD, such as membrane cleaning and dosing of anti-scalants [9-11]. However, these strategies increase either the complexity or cost of MD operation [12]. Very recently, superhydrophobic MD membranes have been explored by several research groups as an effective material strategy for scaling mitigation [13-15]. While the detailed mechanism for scaling-resistance remains an active area of study, these studies collectively show the effectiveness of using superhydrophobic membranes for mitigating mineral scaling in MD [16-18].

A superhydrophobic membrane is a membrane with a very high water contact angle (WCA) and very low contact angle hysteresis. The contact angle hysteresis can be quantified by measuring the sliding angle (SA) which is the minimum tilting angle (from the horizontal position) at which a water droplet starts to slide off the membrane surface. In the convention of material science, both very high WCA (>150 º) and very low SA (<10 º) are required for a surface to be classified as “superhydrophobic” [19, 20]. In other words, a surface with strong contact angle hysteresis (i.e., high SA) is not superhydrophobic, regardless of its WCA.

The two major requirements for fabricating a superhydrophobic membrane, or more

generally, a superhydrophobic surface, are that (1) the material has low surface energy [21, 22], and (2) the surface has a high degree of roughness [23]. Following this principle, most existing superhydrophobic MD membranes were obtained by decorating the surface of commercial hydrophobic membranes with fluorinated nano- or micron-sized particles [24-26]. However, this approach of surface decoration is of limited practical application because (1) the vapor permeability is often significantly compromised with this approach [27-29], and (2) robust attachment of particles onto the membrane surface is challenging and often requires complex, multi-step modification procedure [30, 31]. Therefore, a new way is in need for scalable fabrication of robust superhydrophobic MD membranes without sacrificing the vapor permeability.

Herein, we report a method of fabricating a robust superhydrophobic (r-SH) membrane for MD with both outstanding vapor permeability and scaling resistance. This method is based on the principle of 3D printing, an additive manufacturing approach that creates object by bottom-up, layer-by-layer deposition of the constituting material [32]. This additive manufacturing approach has received increasing recent attention in fabricating membranes and module components. For example, recent studies have been reported to use electrospraying for fabrication of polyamide membranes with exceptional control of active layer thickness and composition [33, 34]. In fact, the many existing studies of using electrospinning to fabricate membranes can all be categorized as additive manufacturing in principle [35]. Notably, electro-co-spinning/spraying (ES^2) has been explored for fabricating fiber/particle composite biomaterials [36, 37].

In this study, we employ an ES^2 method to develop MD membranes with a r-SH layer with micron-sized clusters of silica nanoparticles (SiNPs) intercalated within a matrix of polymeric nanofibers. We characterize the morphological and wetting properties of the r-SH membranes, and also test the MD performance of such r-SH membranes and compare them with conventional hydrophobic membranes and superhydrophobic (SH) membranes obtained using conventional method of decorating surface with fluorinated particles. We also investigate the scaling resistance of the r-SH membranes in MD operation with NaCl and gypsum as the scalants.

MATERIALS AND METHODS

Chemicals and membranes. Polyvinylidenefluoride-co-hexafluoropropylene (PVDF-HFP) (PVDF-HFP, MW: 455 kDa), N,N-dimethylformamide (DMF, 99.8%), acetone (99.9%), sodium chloride (NaCl), 2-propanol (99.5%), 1H,1H,2H,2H -perfluorodecyltriethoxysilane (17-FAS, 97%) were purchased from Sigma-Aldrich (St. Louis, USA). Silica nanoparticles (SiNPs) with 40-60 nm diameter were purchased from SkySpring Nanomaterials (Houston, TX). A commercial polyvinylidene difluoride (PVDF) membrane with 0.45 μm nominal pore size from GE Healthcare (Pittsburg, PA) was used as the reference in scaling experiments.

Fabrication of the r-SH membrane and reference membranes.

The dope solution for electrospinning was prepared by dissolving PVDF-HFP pellets at 20 wt% using a 2:1 (by volume) mixture of DMF to acetone as solvent (mixed overnight at 50°C). The dope solution for electrospraying, referred to as SiNPs/PVDF-HFP dope, was prepared by first dissolving PVDF-HFP pellets to prepare at 8 wt% using a 4:1 (by volume) mixture of DMF to acetone as solvent (mixed overnight at 50°C) and then adding SiNPs (15 wt%) to this solution under vigorous stir-mixing at room temperature for 2 h. Acetone was used to accelerate solvent evaporation during electrospraying, as the already-spun nanofibrous substrate could easily dissolve if only DMF was used as the solvent for the dope solution.

The four-step procedure for fabricating the r-SH membrane is schematically depicted in Figure 1. In step 1, a nanofibrous substrate was electrospun using an electrospinning instrument (TL-01, Tongli Tech., China) by feeding the 20 wt % PVDF-HFP dope solution at 1.0 mL h^{-1}. In step 2, both PVDF-HFP electrospinning dope and SiNPs/PVDF-HFP electrospraying dope were deposited onto the PVDF-HFP fibrous substrate via the electro-co-spinning/spraying (ES^2) technique for 20 min with the spinning and spraying needles facing the rotating collector drum from opposite directions (Figure S1). For the membrane under primary investigation in this paper, flow rate of the SiNPs/PVDF-HFP

electrospraying dope solution was fixed at 2.5 mL h^{-1}, whereas the flow rate of the PVDF-HFP electrospinning dope solution was 0.3 ml h^{-1}. Other flow rates of the PVDF-HFP electrospinning dope solution were also tested and will be discussed later. The low polymer concentration in electrospraying dope solution facilitates the formation of SiNPs/PVDF-HFP microbeads [38, 39]. In both steps, a voltage of 13 kV was applied between the collecting drum rotating at 250 rpm and the needles that reciprocated horizontally at 120 cm min^{-1}.

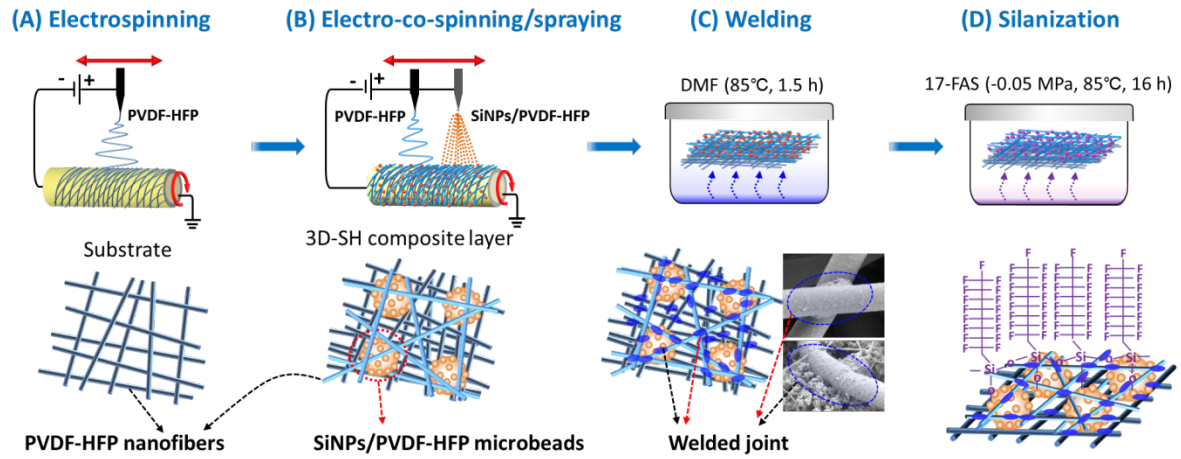

Figure 1. Schematic illustration of the ES^2 procedure for fabricating r-SH membrane. **(A)** Fabrication of the PVDF-HFP nanofibrous substrate by electrospinning. **(B)** Construction of a r-SH composite layer with electrosprayed SiNPs/PVDF-HFP microbeads embedded in electrospun PVDF-HFP fibrous web. **(C)** Structural reinforcement by chemical vapor "welding" using DMF solvent vapor. **(D)** Fluorination of the SiNPs in the membrane structure using 17-FAS via vapor phase silanization.

After the formation of nanofibrous network intercalated with SiNPs/PVDF-HFP microbeads, the fibrous network was subject to DMF vapor phase "welding" at 85 °C for 1.5 h (step 3). The vaporized DMF solvent slightly dissolved the PVDF-HFP on the surface of the fibers and the microbeads, resulting in "welding" of the contact points between fibers themselves and between fibers and the microbeads. This step was performed with the intention to enhance the mechanical integrity of the r-SH membrane. Finally, the welded membrane was functionalized with fluoroalkylsilane (i.e., 17-FAS) to lower the membrane surface energy via vapor phase silanization at 85 °C and -0.05 MPa for 16 h in an vacuum oven (step 4) [17]. The superhydrophobic membrane formed following this stated procedure, as described in Figure 1, is referred to r-SH membrane in the following discussion.

Membrane characterization and performance test

The surface morphology of each membrane was characterized using scanning electron microscopy (SEM, Zeiss Merlin, Thornwood, NY). After scaling experiments,eElemental mapping of the species in the scale layers on the different membranes was conducted with the SEM equipped with energy dispersive X-ray detector, (EDS, Oxford Instruments, Oxfordshire, UK). Static WCA was measured with an optical goniometer (OneAttension, Biolin scientific instrument, Espoo, Finland). We also quantified the WCA hysteresis by measuring the sliding angle, SA. The membrane porosity was measured using a gravimetric method [40]. To quantify the robustness of the membrane wetting properties, the WCA and SA of the membrane samples were measured after the membranes were subjected to prolonged ultrasonic treatments (660 watts, Kendal, China) for 90, 180, 270 minutes.

We evaluated the performance of the membrane samples using a laboratory-scale direct contact membrane distillation (DCMD) system with membrane coupons (2.5 cm × 8 cm). The mass and conductivity of the distillate were measured continuously, from which the real time flux and salt rejection were calculated. For evaluating the intrinsic MD performance in the absence of scaling, we used 2.3 L of NaCl solution (3.5 wt%) as the feed water. The feed and distillate temperatures were 65 and 20 °C, respectively, whereas the cross-flow velocities in the feed and distillate channels were 8.6 and 4.3 cm s^{-1}, respectively.

Scaling resistance evaluation

We performed two sets of experiments with two feed solutions of different chemistry to evaluate the scaling resistance of the different membranes. In the first set of experiments, we used 840 mL of highly concentrated NaCl solution (25 wt%) as the feed water. The feed and distillate temperatures were 60 and 20 °C, respectively, whereas the cross-flow velocities in the feed and distillate channels were 6.5 and 4.3 cm s^{-1}, respectively. In the second set of experiments, the feed solution (initial volume of 840 mL) contained 14 mM $CaCl_2$ and 14 mM Na_2SO_4. The feed and distillate temperatures were 75 and 20 °C, respectively, whereas the cross-flow velocity in the feed and distillate channels was 7.6 and 4.3 cm s^{-1}, respectively. Scaling experiments were terminated when the volume of solution in the feed tank was

insufficient to keep the feed loop free of air bubbles.

RESULTS AND DISCUSSIONS

Membrane morphology

The r-SH membrane displays a rough, porous morphology consisting of SiNPs/PVDF-HFP microbeads (with an average diameter of 11.3±3.1 μm) and intercrossing PVDF-HFP nanofibers (with an average diameter of 420±180 nm) wrapping around the microbeads (Figure 2A). Welding does not only fuse the PVDF-HFP nanofibers at their intercrossing junctions but also fuses the fibers with the SiNPs/PVDF-HFP microbeads. The surface of the SiNPs/PVDF-HFP microbeads exhibits a secondary nanoscale roughness due to the presence of the SiNPs that are "glued" by the PVDF-HFP to become composite microbeads.

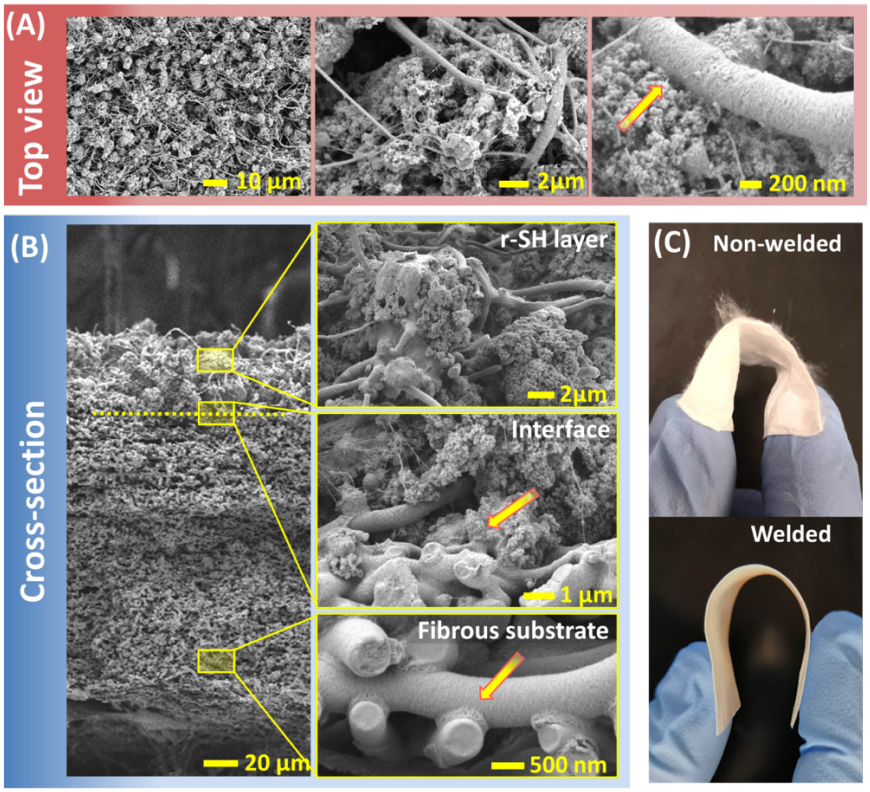

Figure 2. (A) SEM micrographs showing the surface of "welded" r-SH membrane at different magnifications: (left) 500 x, (center) 10,000 x, and (right) 50,000 x. (B) Cross-section morphologies of r-SH membrane. The composite layer (top), the fibrous substrate (bottom), and the boundary between the two layers (center) are highlighted with magnified images shown on the right. (C) Physical appearance of the r-SH membrane before welding (top) and after welding (bottom).

This composite layer with both fibers and microbeads, constructed via ES^2 onto a fibrous PVDF-HFP substrate, forms a robust superhydrophobic layer that is approximately 35 μm thick (Figure 2B left). Higher magnification of the cross-sectional SEM image of the r-SH layer (Figure 2B top right), the interface between the r-SH layer and the fibrous substrate (Figure 2B center right), and the fibrous substrate (Figure 2B bottom right) reveal welding-induced reinforcement within the two respective layers and at their interface. This welding reinforcement is also critical to the mechanical integrity of membranes, i.e., without welding the membranes were flimsy with loose fibers that can be easily peeled away from the substrate (Figure 2C top) because the fibers only physically stack without inter-fiber connection [41-43]; in contrast, the welding-reinforced membranes were significantly more robust (Figure 2C bottom), allowing them to be used in MD as self-supporting membranes without additional mechanical reinforcement. The SEM images of other prepared membranes were also shown in Figure S2 (before welding) and Figure S3 (after welding).

Wetting properties and robustness of the membranes

The membrane wetting properties were compared using WCA and SA with DI water as the testing liquid. All membranes fabricated in this study have higher WCA than that of a commercial PVDF membrane. The WCA increases systematically with a percentage of 17-FAS fluorinated SiNPs/PVDF-HFP microbeads (Figure 3A). The abundance of microbeads was adjusted by controlling the flow rates of the dope solutions in the ES^2 process (Table S1). Both the membrane fabricated via the ES^2 procedure described in the Methods section and the membrane with electro-sprayed composite microbeads (microbeads only) are superhydrophobic, i.e., they both have WCA higher than 150º and SA lower than 10º. In contrast, the SA was not measurable with commercial PVDF membrane and electrospun membranes without microbeads (fibers only), because the water droplet adhered onto the membrane surface even when the membranes were inverted. Expectably, the membrane fabricated using ES^2 with a lower percentage of microbeads (mostly fibers), has a relatively high SA, falling between that of the electrospun membrane (fibers only) and the r-SH membrane formed via ES^2.

Although the membranes formed via ES^2 with both microbeads and fibers and that formed via electrospraying of microbeads (only) are both superhydrophobic right after synthesis, the superhydrophobicity is much more robust with the membrane formed via ES^2. This difference was confirmed by subjecting both membranes to ultrasonication which can potentially "knock" the SiNPs/PVDF-HFP microbeads off the membrane surface. The WCA decreased, and the SA increased, as the membranes with only electrosprayed microbeads experienced longer ultrasonication (Figure 3B). Such a membrane was no longer superhydrophobic after 270 min of ultrasonication, yielding a WCA of only 145.9° and a SA up to 64.0°. In contrast, the ES^2-formed r-SH membrane was only slightly affected by prolonged ultrasonication and remained superhydrophobic after 270 min of ultrasonication. The robustness of superhydrophobicity of ES^2 membrane was further demonstrated in a more practically relevant context where both the electrosprayed SH membrane and the ES^2-derived r-SH membrane membrane was subject to a 30-hour MD experiment with DI water and a cross-flow velocity of 7.6 cm s^{-1}. The WCA and SA of the originally SH membrane with electrosprayed microbeads became 144.8° and >90°, respectively; whereas the WCA and SA of the r-SH membrane were only subject to slight changes to 155.6 º and 7.2 º, respectively. The comparison between these two membranes is qualitatively consistent in both the sonication and prolonged MD experiments.

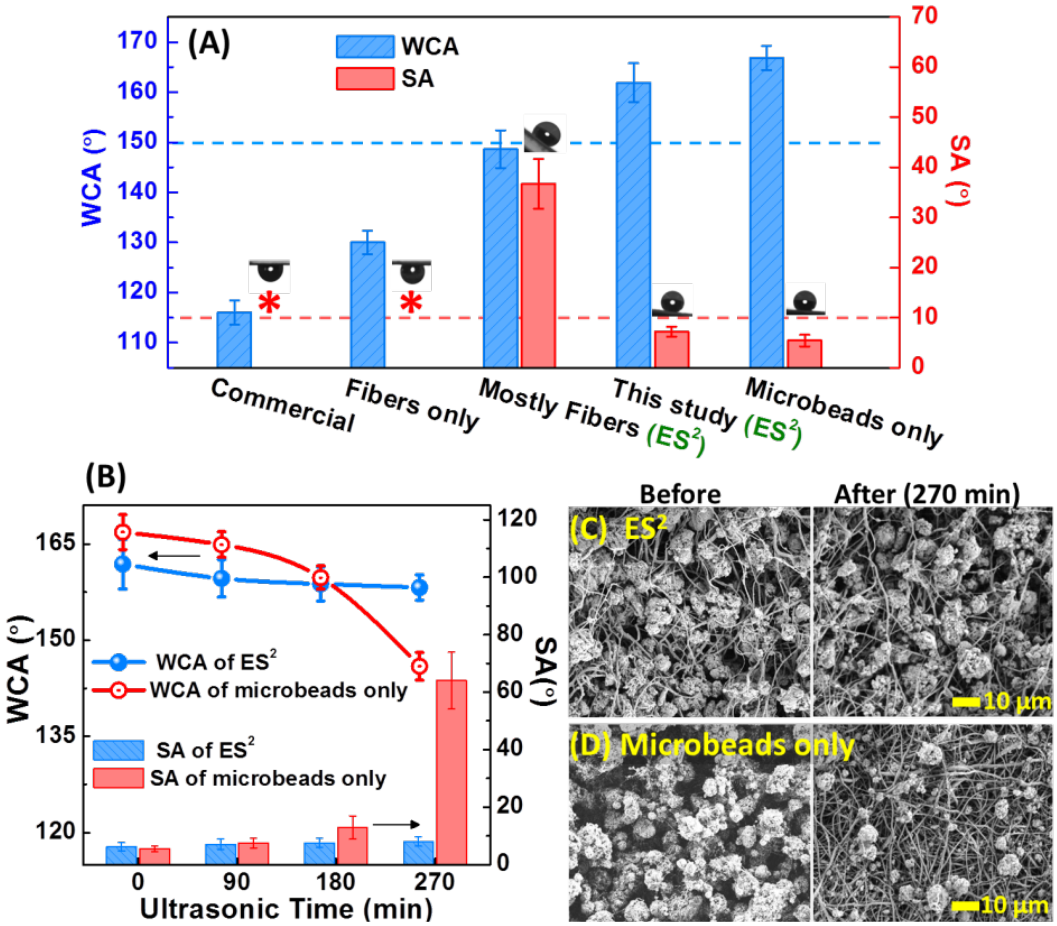

Figure 3. (A) WCA and SA of different membrane samples. The SA of commercial PVDF membrane and the electrospun PVDF-HFP membrane (fibers only) cannot be measured because water droplets adhere even onto an inverted membrane surface. The membrane sample denoted as "mostly fibers" was fabricated also using ES^2 but with a different composition (see Supplementary Information for details). The membrane sample denoted as "microbeads only" was fabricated by electrospraying SiNPs/PVDF-HFP composite beads, without simultaneous electrospinning of PVDF-HFP fibers, onto the already formed PVDF-HFP fibrous substrate. **(B)** WCA and SA of the r-SH membranes fabricated using ES^2 and using electrospraying of SiNPs/PVDF-HFP microbeads after different durations of ultrasonication. **(C)** SEM surface morphology of ES^2-derived r-SH membrane before (left) and after (right) 270 mins of ultrasonication. **(D)** SEM surface morphology of superhydrophobic membrane fabricated by electrospraying SiNPs/PVDF-HFP composite beads before (left) and after (right) 270 mins of ultrasonication.

The robustness of the wetting properties for ES^2-formed r-SH membrane is attributable to the unique structure formed via ES^2 in which composite SiNPs/PVDF-HFP microbeads are locked up in the interconnected network of PVDF-HFP fibers that was further reinforced by the "welding" process. Prolonged ultrasonication was not able to remove the microbeads from such an interconnected and welded network, as evidenced by the lack of change in surface morphology (Figure 3C). In contrast, the surface structure of the membranes with only electrosprayed microbeads is significantly more susceptible to degradation by

ultrasonication because of the weak connections between the microbeads. While the "welding" process may strengthen such connections by fusing the contacting PVDF-HFP portions between different microbeads, this reinforcement was still insufficient when the surface was subject to prolonged perturbation. The layer of SiNPs/PVDF-HFP microbeads was almost completely removed after 270 mins of ultrasonication, as clearly shown by comparing the surface morphology before and after ultrasonication (Figure 3D).

MD performance (in the absence of scaling)

Without the superhydrophobic layer, the electrospun fibrous membrane achieved a vapor flux of 51.1 L m^{-2} h^{-1} (Figure S4) with the feed and distillate temperatures being 65 and 20 °C, respectively. With a superhydrophobic layer constructed by electrosprayed SiNPs/PVDF-HFP microbeads, however, the vapor flux declined to 34.3 L m^{-2} h^{-1} which was similar to that of the commercial PVDF membrane (35. 2 L m^{-2} h^{-1}). This finding is qualitatively consistent with most previous studies that reported a decline in vapor permeability due to the use of a nanoparticle "cake layer" on the membrane surface to impart superhydrophobicity [44-46]. However, using the ES^2 method only led to a much smaller decline of vapor permeability, yielding a vapor flux of 45.6 L m^{-2} h^{-1} with the same experimental conditions. The difference in MD performance between the ES^2-derived r-SH membrane and the superhydrophobic membrane formed via electrospraying microbeads is even more dramatic considering the fact that the functional superhydrophobic layer was 35 μm thick for the ES^2-derived membrane but only 16 μm thick for the membrane with electrosprayed microbeads.

The better MD performance with the thicker ES^2-derived r-SH membrane is mainly attributable to its higher porosity. Compared to electrospun membrane which has the highest porosity of 84.2±0.7 % (Table S2), the ES^2-derived r-SH membrane has a slightly lower overall porosity of 80.7±1.2 %, which is significantly higher than the porosity of membrane with electrosprayed microbeads (69.7±1.5 %). The presence of the co-spun fibers significantly reduces the packing density of the microbeads, preventing the formation of a low-porosity layer that forms with microbeads alone, but at the same time maintains superhydrophobicity. Therefore, both the long-term robustness of superhydrophobicity and

276 the MD performance suggest that r-SH membrane synthesized using ES^2 should be used in
277 MD instead of the superhydrophobic membrane formed only via electrospraying.

278 **Resistance to scaling by NaCl**

279 Experiments with a high concentration NaCl feed solution (25 wt%) show that the
280 electrospun fibrous PVDF-HFP membrane is more scaling resistant than the commercial
281 PVDF membrane (Figure 4A). Specifically, the limiting recovery, defined as the water
282 recovery at which precipitous flux decline occurred, was higher with the fibrous PVDF-HFP
283 membrane (~141 mL,) than with the commercial PVDF membrane (~103 mL). Beyond the
284 limiting recovery, a sharp increase in distillate conductivity was observed for both
285 membranes (Figure 4A), indicating the occurence of scaling-induced pore wetting [15, 47]. In
286 contrast, the r-SH membrane is exceptionally resistant to scaling by NaCl as indicated by the
287 absence of either flux decline or pore wetting even after around 420 mL of water was
288 recovered, and the feed solution was concentrated approximately 2-fold.

289 The observation of sustained vapor flux even when the NaCl feed solution was highly
290 concentrated is similar to what has been reported by Xiao et. al [16] using a templated
291 micropillared superhydrophobic MD membrane, except that in our case we did not even
292 observe any increase in distillate conductivity as reported by Xiao et al. [16], even when the
293 feed water was concentrated by more than 2-fold. This exceptional resistance to scaling and
294 the pore wetting thereby-induced may be attributable to the r-SH layer that is dramatically
295 more difficult to penetrate than membranes that rendered superhydrophobic only by surface
296 features [48, 49].

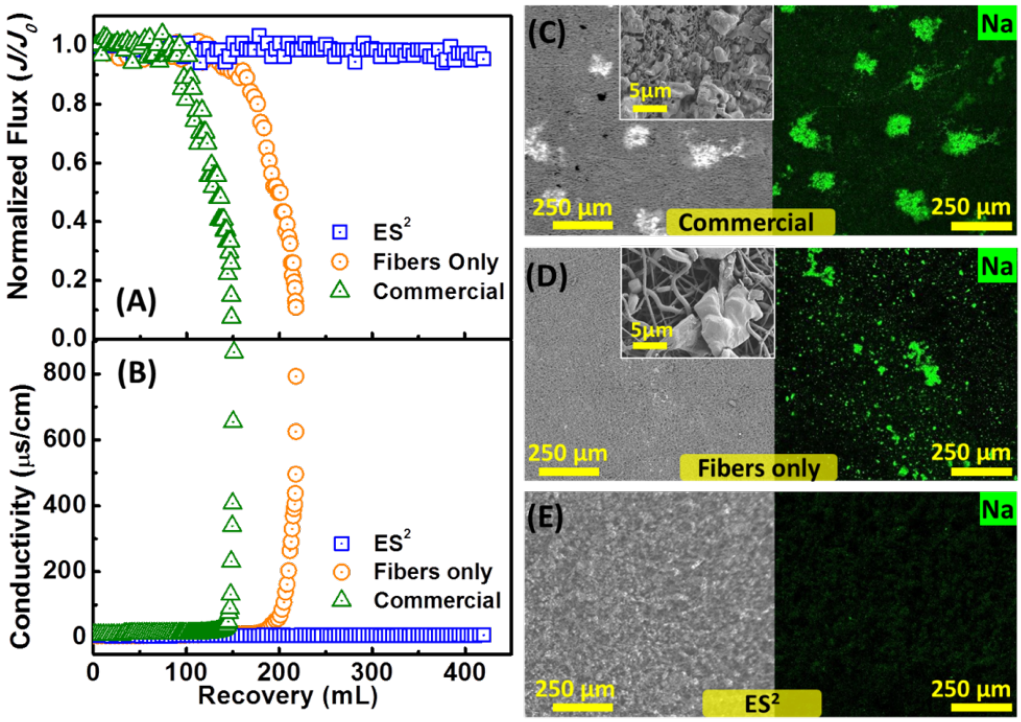

Figure 4. **(A)** Normalized water flux and **(B)** distillate conductivity as functions of the water recovery for r-SH membrane fabricated using ES^2 (blue), electrospun PVDF-HFP membrane (orange), and commercial PVDF membrane (green) in NaCl scaling experiments (the replicates of the results shown in A and B are also presented in Figure S5). The average initial vapor fluxes for the three membranes were 27.4 L, 28.5, and 16.2 m^{-2} h^{-1}, respectively, with a feed temperature of 60 °C and a distillate temperature of 20 °C. The feed water was 840 mL NaCl solution (25 wt %). SEM micrographs (left) and the corresponding EDS mapping for Na element (right) for **(C)** commercial PVDF membrane, **(D)** electrospun PVDF-HFP fibrous membrane, and **(E)** r-SH membrane fabricated using ES^2.

The fact that both the electrospun fibrous membrane and the r-SH membrane had significantly higher water fluxes than the commercial PVDF membrane suggests that the observed difference in scaling behaviors has little to deal with concentration polarization, as otherwise the electrospun membrane and the r-SH membrane should have had lower limiting recoveries than the commercial PVDF membrane that had the lowest vapor flux. Top-view SEM images and the corresponding EDS mapping of Na element reveal large NaCl crystal on the surface the commercial PVDF membrane (Figure 4C) and significantly smaller crystals on the electrospun PVDF-HFP membrane (Figure 4D) after the scaling experiments. In contrast, very little Na was detected on the r-SH membrane, and no observable crystal was found on the surface of the r-SH membrane at all.

We also measured the WCA and SA of the three membrane samples after scaling experiments (without rinsing) and found that whereas the WCA of the commercial PVDF

membrane and the electrospun PVDF-HFP membrane decreased by 29.7 and 19.9°, respectively (Figure S6). The decreased hydrophobicity of these membranes may be attributable to the presence of surface-bound crystal deposit. In contrast, the WCA of the r-SH membrane decreased by only 4.6º to 157º. Besides, the WCA hysteresis for the r-SH membrane remained very small, as quantified by a SA of 9.0° even after the scaling experiments (Figure S6). In conclusion, the wetting properties of the r-SH were almost unaffected by the scaling experiment with highly concentrated NaCl solution, again confirming the robustness of its superhydrophobicity.

Resistance to scaling by gypsum

The scaling behavior with gypsum, a sparely soluble mineral, differs substantially from that with NaCl. With the commercial PVDF membrane and the electrospun PVDF-HFP membrane, the flux decline upon the onset of scaling is less "precipitous" with gypsum scaling than with NaCl scaling. Based on the water recovery corresponding to the onset of scaling and the flux decline rate, the r-SH membrane was more scaling resistant than the commercial or electrospun membranes (Figure 5A, 5B). However, unlike the case with concentrated NaCl solution as feedwater, even the r-SH membrane was subject to gypsum scaling that leads to both flux decline and pore wetting. This observation is consistent with recent studies using superhydrophobic membranes in MD, that superhydrophobic membrane can only delay, but not eliminate gypsum scaling [15, 17, 50]. The exact mechanism underlying these different scaling behaviors between NaCl and gypsum is beyond the scope of this study and needs further elucidation. But it is nonetheless consistent with the observations in a recent study by Xiao et al [16, 50].

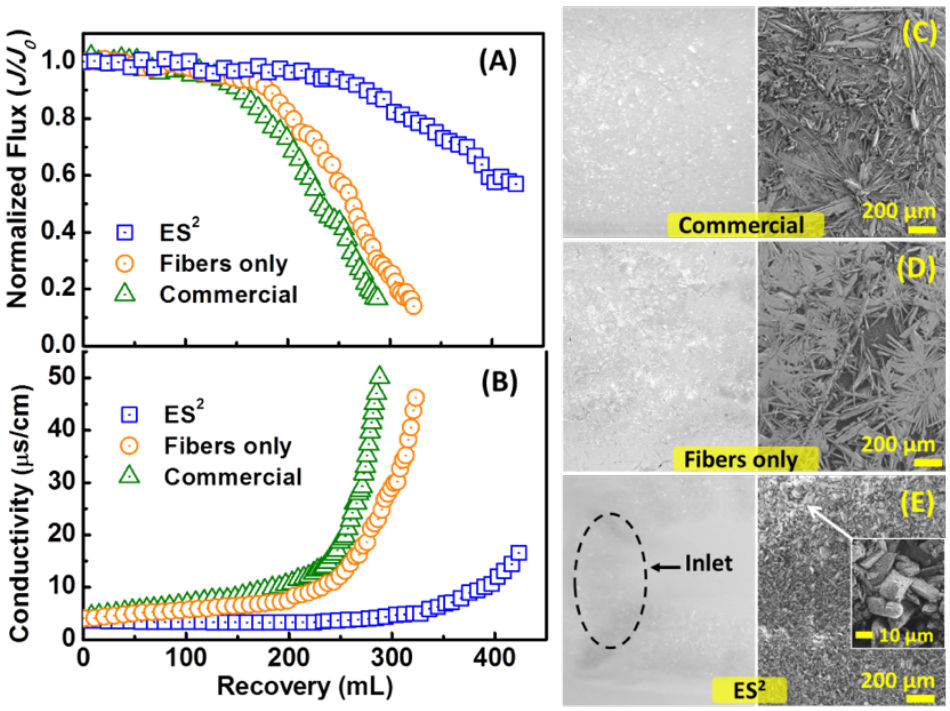

Figure 5. **(A)** Normalized water flux and **(B)** distillate conductivity as functions of the water recovery for r-SH membrane fabricated using ES^2 (blue), electrospun PVDF-HFP membrane (orange), and commercial PVDF membrane (green) in gypsum scaling experiments (the replicates of the results shown in A and B are also presented in Figure S7). The average initial vapor fluxes for the three membranes were 44.5, 48.1, and 40.2 L m^{-2} h^{-1}, respectively, with a feed temperature of 75 °C and a distillate temperature of 20 °C. The feed water was 840 mL of a mixed 14 mM/L $CaCl_2$ and 14 mM/L Na_2SO_4 solution. Photographic images (left) and SEM micrographs (right) for **(C)** commercial PVDF membrane, **(D)** electrospun PVDF-HFP membrane, and **(E)** r-SH membrane fabricated using ES^2.

Results from membrane autopsy also indicate that gypsum scaling on the r-SH membrane is qualitatively different from that on the commercial PVDF membrane or the electrospun PVDF-HFP membrane. With hydrophobic (but not superhydrophobic) membranes, needle-like gypsum crystals almost entirely covered the membrane surface (Figure 5C, 5D). With a r-SH membrane, however, a large fraction of the membrane surface remained free of scaling crystals. Interestingly, the portions of the r-SH membrane that were covered by gypsum crystal were either near the entrance and exit or along the edges of the feed channel (Figure S8). Because the hydrodynamic conditions in these regions are more stagnant than that in the central region of feed channel, it is most likely that hydrodynamic effect plays an important role in mitigating gypsum scaling on the superhydrophobic membrane [16]. Scaling near the entrance seems to be the most severe among all regions likely due to additional conditions that are favorable for crystal precipitation. Specifically, the higher feed temperature at the entrance leads to both lower gypsum solubility [51] and stronger concentration polarization as a result of high vapor flux [52, 53]. Perhaps more importantly, the

feed stream near the entrance has a flow component toward the membrane surface, which enhances the convective transport of solutes toward the membrane surface.

Mechanisms for scaling mitigation with superhydrophobic membrane

It is widely believed that an air layer is present on the surface of a superhydrophobic membrane submerged in water [54-56]. The presence of such a surface-bound air layer on a superhydrophobic membrane is evidenced by the silvery and reflective appearance of the submerged surface, which is caused by the different refractive indexes between water and air [57-60] (Figure 6A). Based on the presence of such an air layer, three possible mechanisms likely contribute to the lower scaling propensity with superhydrophobic membranes, even though their relative contributions are difficult to quantify.

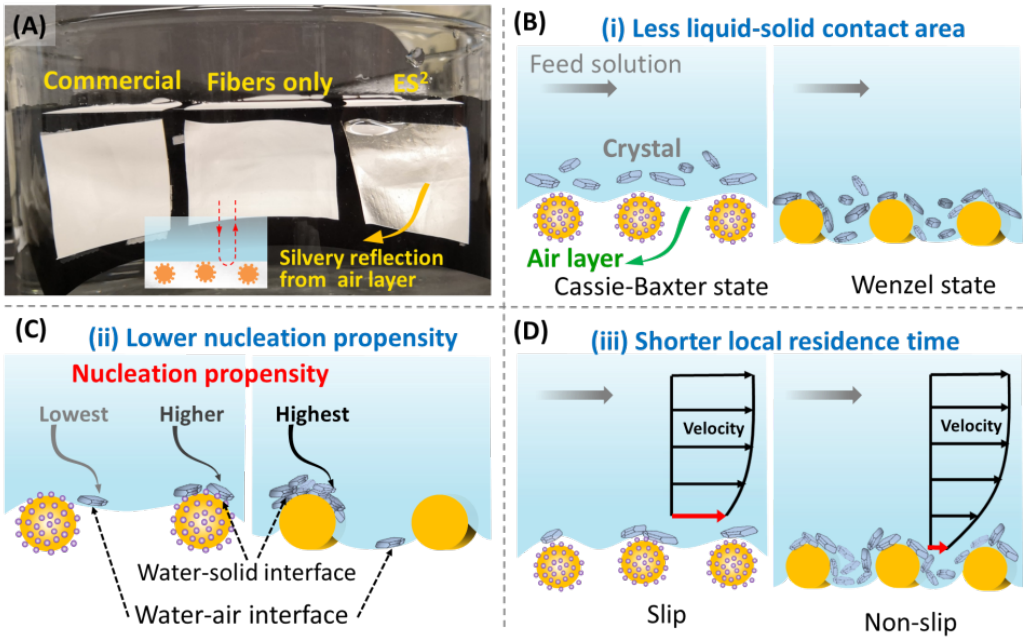

Figure 6. (A) Photographic image of the submerged commercial PVDF membrane (left), electrospun PVDF-HFP fibrous membrane (center), and r-SH membrane fabricated using ES^2 (right). The r-SH membrane has a silvery reflective surface due to the presence of a surface-bound air layer. Graphical illustration of **(B)** reduced liquid-solid interfacial area, **(C)** lower overall surface energy and nucleation propensity, and **(D)** reduced local residence time, with a superhydrophobic membrane (left) as compared with a hydrophobic membrane (right).

The first mechanism is the reduced liquid-solid contact area, which is consequent of the excellent Cassie-Baxter state required for superhydrophobicity. The smaller contact area between the feed solution and the solid material of the membrane reduces the area of

interfacial crystallization at the water-solid interface and thereby reduces the overall adhesive interaction between the scale layer and the MD membrane (Figure 6B). A recent paper by Horseman et al. also suggests the formation of crystal "anchors" within the membrane pores when the feed solution partially intrudes into a conventional hydrophobic MD membrane [61]. Such an anchoring effect can be minimized with superhydrophobic membranes with minimum pinning as indicated by a very low sliding angle. In addition, this mechanism also contributes to less deposition of crystal particles that are heterogeneously formed in the bulk, simply because small area of solid-water interface is available for particle deposition.

While the first mechanism regards the reduced area for interaction between crystals and the membrane, the second mechanism concerns the more difficult formation of such crystals on superhydrophobic membranes than on hydrophobic membranes. It is widely accepted that heterogeneous nucleation at the solid-water interface is typically more favorable and faster than homogeneous nucleation [62, 63]. Interestingly, previous analyses also showed that the Gibbs free energy for heterogeneous nucleation at water-air interface equals that for homogeneous nucleation [64, 65]. Since surface energy of air is practically zero and the surface energy of 17-FAS is lower than that of PVDF (and PVDF-HFP), the ranking of "nucleation propensity" should follow the order below:

$$\text{PVDF} > \text{17-FAS} > \text{Water-air interface} \sim \text{Homogeneous nucleation}$$

If we divide the total contact area between feed solution and the membrane into two fractions with one being water-air contact and the other being the water-solid contact, MD with superhydrophobic membrane has a larger fraction of water-air contact which has the lowest nucleation propensity. Furthermore, even for the portion of water-solid contact, the lower surface energy of the 17-FAS on a superhydrophobic membrane also results in a lower scaling propensity than with a PVDF (and PVDF-HFP) hydrophobic membrane. Both effects cooperatively lead to more difficult nucleation on a superhydrophobic than on a hydrophobic membrane (Figure 6C).

The third mechanism is related to the reduced local residence time available for interaction between mineral ions and the solid surface of the membrane. The air layer

between a superhydrophobic surface and the fluid flowing along it is effective in reducing the drag to fluid flow due to what has been referred to as the "slip boundary effect" [66]. Unlike typical non-slip boundary at which the local flow velocity is considered to be zero at the solid-water interface, the flow velocity at a slip boundary is positive (Figure 6D) [57, 67, 68]. For a non-permeable solid surface, the higher flow velocity on a superhydrophobic surface with slip-boundary leads to significantly less residence time for interaction between mineral ions and surface, which reduces the scaling propensity. For a permeable surface like a membrane, the impact of local residence time is all the more significant. The potentially significantly longer residence time is caused by the partial intrusion of feed solution into the pores of a hydrophobic membrane creates a stagnant zone within the pore where mineral ions can linger (Figure 6D). This effect may be exacerbated by convective transport into this stagnant zone due to vapor flux in MD. The detrimental impact of the slip-boundary and in-pore stagnant zone applies to both interfacial heterogeneous nucleation and deposition of crystal particles that have already formed in the solution.

In summary, the recently proposed strategy of using superhydrophobic membranes for scaling mitigation has three possible mechanisms including reduced solid-water contact area for interaction of the membrane surface with crystal particles or solutes, lower nucleation propensity due to the reduced overall surface energy, and the shorter local residence time for interaction between mineral ions and solid surface. These mechanisms, which result from the exceptional Cassie-Baxter state imparted by superhydrophobic membranes, likely all contribute to the effectiveness of superhydrophobic membrane for universally reducing the propensity of mineral scaling. However, breaking down individual contributions of these mechanisms is both experimentally and theoretically challenging.

IMPLICATIONS

As a thermal distillation process that is inherently energy intensive, the most promising applications of MD are treatment of hypersaline brine, which is an emerging environmental challenge with growing importance. To unlock the potential of MD toward its best-suited applications, the critical challenge of mineral scaling must be overcome. While recent

research has demonstrated the potential of superhydrophobic membranes in mitigating mineral scaling in MD, the method reported herein for fabricating three-dimensionally superhydrophobic (r-SH) membrane using electro-co-spinning/spraying (ES^2) offers a scalable approach for making superhydrophobic membrane with robust superhydrophobicity and minimal compromise in the intrinsic MD performance. To the best of our knowledge, the r-SH membrane fabricated using ES^2 delivers higher flux than most, if not all, superhydrophobic membranes reported in other studies with similar operating conditions. The unique particles-in-fibrous-web structure of the r-SH membrane also delivers highly robust superhydrophobicity that is required for stable performance in long-term operations.

ASSOCIATED CONTENT

Supporting Information

Fabrication and composite of reference membranes (Table S1); schematic (top and side views) of the ES^2 process (Figure S1); SEM images of the membranes before (Figure S2) and after welding (Figure S3); thickness and porosity of the membranes (Table S2); water flux and solution conductivity of the membranes using a 3.5wt% NaCl as feed solution (Figure S5); photo of membranes surface (feed side) after scaled by 25 wt % NaCl (Figure S6); reproducible DCMD results for concentrating the 25 wt % NaCl (Figure S7) and $CaSO_4$ feed solution (Figure S8).

AUTHOR INFORMATION

Corresponding Author

E-mail:ypli@ipe.ac.cn Phone: + 86 1082544839. (Y. L.)

E-mail:shihong.lin@vanderbilt.edu. Phone: +1 (615) 322-7226. (S.L.)

Notes

The authors declare no competing financial interest.

ORCID

Chunlei Su: 0000-0002-6732-9455

Thomas Horseman: 0000-0002-4660-1448

Yuping Li: 0000-0003-2490-0436

Shihong Lin: 0000-0001-9832-9127

ACKNOWLEDGMENTS

C.S. is thankful to the support from China Scholarship Council (No.201804910753); T.H. is supported by American Chemical Society Petroleum Research Foundation via grant ACS-PRF 57353 DNI; K.C. acknowledges the support from National Science Foundation via an NSF-GRFP award DGE-1145194; and S.L. acknowledges the support from National Science Foundation via standard research grant 1705048.

REFERENCES

1. Deshmukh, A.; Boo, C.; Karanikola, V.; Lin, S.; Straub, A. P.; Tong, T.; Warsinger, D. M.; Elimelech, M., Membrane distillation at the water-energy nexus: limits, opportunities, and challenges. *Energy Environ. Sci.* **2018,** *11*, (5), 1177-1196.

2. Lin, S.; Yip, N. Y.; Elimelech, M., Direct contact membrane distillation with heat recovery: Thermodynamic insights from module scale modeling. *J. Membr. Sci.* **2014,** *453*, (0), 498-515.

3. Wang, Z.; Jin, J.; Hou, D.; Lin, S., Tailoring surface charge and wetting property for robust oil-fouling mitigation in membrane distillation. *J. Membr. Sci.* **2016,** *516*, 113-122.

4. Su, C.; Li, Y.; Cao, H.; Lu, C.; Li, Y.; Chang, J.; Duan, F., Novel PTFE hollow fiber membrane fabricated by emulsion electrospinning and sintering for membrane distillation. *J. Membr. Sci.* **2019,** *583*, 200-208.

5. Su, C.; Lu, C.; Cao, H.; Gao, F.; Chang, J.; Li, Y.; He, C., Fabrication of a novel nanofibers-covered hollow fiber membrane via continuous electrospinning with non-rotational collectors. *Mater. Lett.* **2017,** *204*, 8-11.

6. Chen, Y.; Zheng, R.; Wang, J.; Liu, Y.; Wang, Y.; Li, X.-M.; He, T., Laminated PTFE membranes to enhance the performance in direct contact membrane distillation for high salinity solution. *Desalination* **2017,** *424*, 140-148.

7. Tian, M.; Yin, Y.; Yang, C.; Zhao, B.; Song, J.; Liu, J.; Li, X.-M.; He, T., CF4 plasma modified highly interconnective porous polysulfone membranes for direct contact membrane distillation (DCMD). *Desalination* **2015,** *369*, 105-114.

8. Tijing, L. D.; Woo, Y. C.; Choi, J.-S.; Lee, S.; Kim, S.-H.; Shon, H. K., Fouling and its control in membrane distillation—A review. *J. Membr. Sci.* **2015,** *475*, 215-244.

9. Turek, M.; Mitko, K.; Piotrowski, K.; Dydo, P.; Laskowska, E.; Jakóbik-Kolon, A., Prospects for high water recovery membrane desalination. *Desalination* **2017,** *401*, 180-189.

10. He, F.; Sirkar, K. K.; Gilron, J., Effects of antiscalants to mitigate membrane scaling by direct contact membrane distillation. *J. Membr. Sci.* **2009,** *345*, (1-2), 53-58.

11. Alkhudhiri, A.; Darwish, N.; Hilal, N., Membrane distillation: A comprehensive review. *Desalination* **2012,** *287*, 2-18.
12. Tong, T.; Wallace, A. F.; Zhao, S.; Wang, Z., Mineral scaling in membrane desalination: Mechanisms, mitigation strategies, and feasibility of scaling-resistant membranes. *J. Membr. Sci.* **2019,** *579*, 52-69.
13. Zhao, F.; Ma, Z.; Xiao, K.; Xiang, C.; Wang, H.; Huang, X.; Liang, S., Hierarchically textured superhydrophobic polyvinylidene fluoride membrane fabricated via nanocasting for enhanced membrane distillation performance. *Desalination* **2018,** *443*, 228-236.
14. Dong, Y.; Ma, L.; Tang, C. Y.; Yang, F.; Quan, X.; Jassby, D.; Zaworotko, M. J.; Guiver, M. D., Stable Superhydrophobic Ceramic-Based Carbon Nanotube Composite Desalination Membranes. *Nano Lett.* **2018,** *18*, (9), 5514-5521.
15. Meng, S.; Ye, Y.; Mansouri, J.; Chen, V., Crystallization behavior of salts during membrane distillation with hydrophobic and superhydrophobic capillary membranes. *J. Membr. Sci.* **2015,** *473*, 165-176.
16. Xiao, Z.; Zheng, R.; Liu, Y.; He, H.; Yuan, X.; Ji, Y.; Li, D.; Yin, H.; Zhang, Y.; Li, X. M.; He, T., Slippery for scaling resistance in membrane distillation: A novel porous micropillared superhydrophobic surface. *Water Res.* **2019,** *155*, 152-161.
17. Karanikola, V.; Boo, C.; Rolf, J.; Elimelech, M., Engineered Slippery Surface to Mitigate Gypsum Scaling in Membrane Distillation for Treatment of Hypersaline Industrial Wastewaters. *Environ. Sci. Technol.* **2018,** *52*, (24), 14362-14370.
18. Wang, Y.; He, G.; Shao, Y.; Zhang, D.; Ruan, X.; Xiao, W.; Li, X.; Wu, X.; Jiang, X., Enhanced performance of superhydrophobic polypropylene membrane with modified antifouling surface for high salinity water treatment. *Sep. Purif. Technol.* **2019,** *214*, 11-20.
19. Tian, X.; Verho, T.; Ras, R. H. A., Moving superhydrophobic surfaces toward real-world applications. *Science* **2016,** *352*, (6282), 142-143.
20. Quan, Y. Y.; Zhang, L. Z.; Qi, R. H.; Cai, R. R., Self-cleaning of Surfaces: the Role of Surface Wettability and Dust Types. *Sci. Rep.* **2016,** *6*, 38239.
21. Yang, C.; Tian, M.; Xie, Y.; Li, X.-M.; Zhao, B.; He, T.; Liu, J., Effective evaporation of CF4 plasma modified PVDF membranes in direct contact membrane distillation. *J. Membr. Sci.* **2015,** *482*, 25-32.
22. Yang, C.; Li, X.-M.; Gilron, J.; Kong, D.-f.; Yin, Y.; Oren, Y.; Linder, C.; He, T., CF4 plasma-modified superhydrophobic PVDF membranes for direct contact membrane distillation. *J. Membr. Sci.* **2014,** *456*, 155-161.
23. Tuteja, A.; Choi, W.; Ma, M.; Mabry, J. M.; Mazzella, S. A.; Rutledge, G. C.; McKinley, G. H.; Cohen, R. E., Designing Superoleophobic Surfaces. *Science* **2007,** *318*, (5856), 1618-1622.
24. Zhang, C.; Yuan, X.; Wu, L.; Han, Y.; Sheng, J., Study on morphology of electrospun poly(vinyl alcohol) mats. *Eur. Polym. J.* **2005,** *41*, (3), 423-432.
25. Meng, S.; Ye, Y.; Mansouri, J.; Chen, V., Fouling and crystallisation behaviour of superhydrophobic nano-composite PVDF membranes in direct contact membrane distillation. *J. Membr. Sci.* **2014,** *463*, 102-112.
26. Hamzah, N.; Leo, C. P.; Ooi, B. S., Superhydrophobic PVDF/TiO2-SiO2 Membrane with Hierarchical Roughness in Membrane Distillation for Water Recovery from Phenolic Rich Solution Containing Surfactant. *Chin. J. Polym. Sci.* **2019,** *37*, (6), 609-616.
27. Dong, Z.-Q.; Ma, X.-H.; Xu, Z.-L.; Gu, Z.-Y., Superhydrophobic modification of PVDF-SiO2 electrospun nanofiber membranes for vacuum membrane distillation. *RSC Advances* **2015,** *5*, (83), 67962-67970.
28. Meng, S.; Mansouri, J.; Ye, Y.; Chen, V., Effect of templating agents on the properties and membrane distillation performance of TiO2-coated PVDF membranes. *J. Membr. Sci.* **2014,** *450*, 48-59.
29. Ardeshiri, F.; Salehi, S.; Peyravi, M.; Jahanshahi, M.; Amiri, A.; Rad, A. S., PVDF membrane assisted by

modified hydrophobic ZnO nanoparticle for membrane distillation. *Asia-Pac. J. Chem. Eng.* **2018,** *13*, (3), e2196.

30. Lu, Y.; Sathasivam, S.; Song, J.; Crick, C. R.; Carmalt, C. J.; Parkin, I. P., Robust self-cleaning surfaces that function when exposed to either air or oil. *Science* **2015,** *347*, (6226), 1132-1135.

31. Im, M.; Im, H.; Lee, J.-H.; Yoon, J.-B.; Choi, Y.-K., A robust superhydrophobic and superoleophobic surface with inverse-trapezoidal microstructures on a large transparent flexible substrate. *Soft Matter* **2010,** *6*, (7), 1401.

32. Low, Z.-X.; Chua, Y. T.; Ray, B. M.; Mattia, D.; Metcalfe, I. S.; Patterson, D. A., Perspective on 3D printing of separation membranes and comparison to related unconventional fabrication techniques. *J. Membr. Sci.* **2017,** *523*, 596-613.

33. Chowdhury, M. R.; Steffes, J.; Huey, B. D.; McCutcheon, J. R., 3D printed polyamide membranes for desalination. *Science* **2018,** *361*, (6403), 682.

34. Ma, X.-H.; Yang, Z.; Yao, Z.-K.; Guo, H.; Xu, Z.-L.; Tang, C. Y., Interfacial Polymerization with Electrosprayed Microdroplets: Toward Controllable and Ultrathin Polyamide Membranes. *Environ. Sci. Technol. Lett.* **2018,** *5*, (2), 117-122.

35. Ahmed, F. E.; Lalia, B. S.; Hashaikeh, R., A review on electrospinning for membrane fabrication: Challenges and applications. *Desalination* **2015,** *356*, 15-30.

36. Zamani, M.; Prabhakaran, M. P.; Ramakrishna, S., Advances in drug delivery via electrospun and electrosprayed nanomaterials. *Int J Nanomedicine* **2013,** *8*, 2997-3017.

37. Ekaputra, A. K.; Prestwich, G. D.; Cool, S. M.; Hutmacher, D. W., Combining Electrospun Scaffolds with Electrosprayed Hydrogels Leads to Three-Dimensional Cellularization of Hybrid Constructs. *Biomacromolecules* **2008,** *9*, (8), 2097-2103.

38. Liao, Y.; Wang, R.; Fane, A. G., Fabrication of Bioinspired Composite Nanofiber Membranes with Robust Superhydrophobicity for Direct Contact Membrane Distillation. *Environ. Sci. Technol.* **2014,** *48*, (11), 6335-6341.

39. Wang, S.; Li, Y. P.; Fei, X. L.; Sun, M.; Zhang, C. Q.; Li, Y.; Yang, Q.; Hong, X., Preparation of a durable superhydrophobic membrane by electrospinning poly (vinylidene fluoride) (PVDF) mixed with epoxy–siloxane modified SiO2 nanoparticles: A possible route to superhydrophobic surfaces with low water sliding angle and high water contact angle. *J. Colloid Interface Sci.* **2011,** *359*, (2), 380-388.

40. Nejati, S.; Boo, C.; Osuji, C. O.; Elimelech, M., Engineering flat sheet microporous PVDF films for membrane distillation. *J. Membr. Sci.* **2015,** *492*, 355-363.

41. Reneker, D. H.; Yarin, A. L.; Fong, H.; Koombhongse, S., Bending instability of electrically charged liquid jets of polymer solutions in electrospinning. *J. Appl. Phys.* **2000,** *87*, (9), 4531-4547.

42. Lalia, B. S.; Guillen-Burrieza, E.; Arafat, H. A.; Hashaikeh, R., Fabrication and characterization of polyvinylidenefluoride-co-hexafluoropropylene (PVDF-HFP) electrospun membranes for direct contact membrane distillation. *J. Membr. Sci.* **2013,** *428*, 104-115.

43. Shaulsky, E.; Nejati, S.; Boo, C.; Perreault, F.; Osuji, C. O.; Elimelech, M., Post-fabrication modification of electrospun nanofiber mats with polymer coating for membrane distillation applications. *J. Membr. Sci.* **2017,** *530*, 158-165.

44. Zhang, J.; Song, Z. Y.; Li, B.; Wang, Q.; Wang, S. C., Fabrication and characterization of superhydrophobic poly (vinylidene fluoride) membrane for direct contact membrane distillation. *Desalination* **2013,** *324*, (0), 1-9.

45. Liao, Y.; Wang, R.; Fane, A. G., Engineering superhydrophobic surface on poly(vinylidene fluoride) nanofiber membranes for direct contact membrane distillation. *J. Membr. Sci.* **2013,** *440*, (0), 77-87.

46. Lee, E.-J.; Deka, B. J.; An, A. K., Reinforced superhydrophobic membrane coated with aerogel-assisted polymeric microspheres for membrane distillation. *J. Membr. Sci.* **2019,** *573*, 570-578.
47. Rezaei, M.; Warsinger, D. M.; Lienhard V, J. H.; Duke, M. C.; Matsuura, T.; Samhaber, W. M., Wetting phenomena in membrane distillation: Mechanisms, reversal, and prevention. *Water Res.* **2018,** *139*, 329-352.
48. Yohe, S. T.; Freedman, J. D.; Falde, E. J.; Colson, Y. L.; Grinstaff, M. W., A Mechanistic Study of Wetting Superhydrophobic Porous 3D Meshes. *Adv. Funct. Mater.* **2013,** *23*, (29), 3628-3637.
49. Liao, Y.; Loh, C. H.; Wang, R.; Fane, A. G., Electrospun Superhydrophobic Membranes with Unique Structures for Membrane Distillation. *ACS Appl. Mat. Interfaces* **2014,** *6*, (18), 16035-16048.
50. Xiao, Z.; Li, Z.; Guo, H.; Liu, Y.; Wang, Y.; Yin, H.; Li, X.; Song, J.; Nghiem, L. D.; He, T., Scaling mitigation in membrane distillation: From superhydrophobic to slippery. *Desalination* **2019,** *466*, 36-43.
51. Nghiem, L. D.; Cath, T., A scaling mitigation approach during direct contact membrane distillation. *Sep. Purif. Technol.* **2011,** *80*, (2), 315-322.
52. Warsinger, D. M.; Tow, E. W.; Swaminathan, J.; Lienhard V, J. H., Theoretical framework for predicting inorganic fouling in membrane distillation and experimental validation with calcium sulfate. *J. Membr. Sci.* **2017,** *528*, 381-390.
53. He, F.; Gilron, J.; Lee, H.; Song, L.; Sirkar, K. K., Potential for scaling by sparingly soluble salts in crossflow DCMD. *J. Membr. Sci.* **2008,** *311*, (1-2), 68-80.
54. Luo, C.; Zheng, H.; Wang, L.; Fang, H.; Hu, J.; Fan, C.; Cao, Y.; Wang, J., Direct three-dimensional imaging of the buried interfaces between water and superhydrophobic surfaces. *Angew. Chem. Int. Ed. Engl.* **2010,** *49*, (48), 9145-8.
55. Yohe, S. T.; Herrera, V. L. M.; Colson, Y. L.; Grinstaff, M. W., 3D superhydrophobic electrospun meshes as reinforcement materials for sustained local drug delivery against colorectal cancer cells. *J. Control. Release* **2012,** *162*, (1), 92-101.
56. Patankar, N. A., Thermodynamics of Trapping Gases for Underwater Superhydrophobicity. *Langmuir* **2016,** *32*, (27), 7023-8.
57. Kavalenka, M. N.; Vullers, F.; Lischker, S.; Zeiger, C.; Hopf, A.; Rohrig, M.; Rapp, B. E.; Worgull, M.; Holscher, H., Bioinspired air-retaining nanofur for drag reduction. *ACS Appl. Mat. Interfaces* **2015,** *7*, (20), 10651-5.
58. Balmert, A.; Bohn, H. F.; Ditsche-Kuru, P.; Barthlott, W., Dry under water: Comparative morphology and functional aspects of air-retaining insect surfaces. *J. Morphol.* **2011,** *272*, (4), 442-451.
59. Babu, D. J.; Mail, M.; Barthlott, W.; Schneider, J. J., Superhydrophobic Vertically Aligned Carbon Nanotubes for Biomimetic Air Retention under Water (Salvinia Effect). *Adv. Funct. Mater.* **2017,** *4*, (13), 1700273.
60. Nguyen, D. D.; Tai, N.-H.; Lee, S.-B.; Kuo, W.-S., Superhydrophobic and superoleophilic properties of graphene-based sponges fabricated using a facile dip coating method. *Environ. Sci. Technol.* **2012,** *5*, (7), 7908-7912.
61. Horseman, T.; Su, C.; Christie, K. S. S.; Lin, S., Highly Effective Scaling Mitigation in Membrane Distillation Using a Superhydrophobic Membrane with Gas Purging. *Environ. Sci. Technol. Lett.* **2019**.
62. Liu, X. Y., Heterogeneous nucleation or homogeneous nucleation? *J. Chem. Phys.* **2000,** *112*, (22), 9949-9955.
63. Sear, R. P., Heterogeneous and Homogeneous Nucleation Compared: Rapid Nucleation on Microscopic Impurities. *J. Phys. Chem. B* **2006,** *110*, (10), 4985-4989.
64. Christenson, H. K., Two-step crystal nucleation via capillary condensation. *CrystEngComm* **2013,** *15*, (11), 2030.

631 65. Kashchiev, D.; Firoozabadi, A., Nucleation of gas hydrates. *J. Cryst. Growth* **2002,** *243*, (3), 476-489.
632 66. McHale, G.; Newton, M. I.; Shirtcliffe, N. J., Immersed superhydrophobic surfaces: Gas exchange, slip and
633 drag reduction properties. *Soft Matter* **2010,** *6*, (4), 714-719.
634 67. Choi, C. H.; Kim, C. J., Large slip of aqueous liquid flow over a nanoengineered superhydrophobic surface.
635 *Phys. Rev. Lett.* **2006,** *96*, (6), 066001.
636 68. Lee, C.; Choi, C.-H.; Kim, C.-J., Superhydrophobic drag reduction in laminar flows: a critical review. *Exp.*
637 *Fluids* **2016,** *57*, (12), 176.

638

639 ## TOC ART

640